Range-Adaptive Wireless Power Transfer Based on Differential Coupling using Multiple Bi-directional Coils

Y. Zhuang, A. Chen, C. Xu, Y. Huang, *Senior Member*, *IEEE*, H. Zhao and J. Zhou

***Abstract*— Wireless power transfer systems using coupled magnetic resonances are susceptible to the transfer distance variation between the transmitter (Tx) and receiver (Rx) since the coupling between Tx and Rx is highly position-dependent. Once the transfer distance deviates from the optimum one, the coupling will be either excessive or weak which results in power transfer efficiency (PTE) degradation. This paper presents a Tx structure consisting of multiple sub-coils oriented in opposite directions to keep the coupling relatively constant over an extensive range of transfer distances. The proposed design can achieve a PTE of 88% - 70% with a transfer distance varying from 0 mm to 70 mm and a PTE of 85% - 60% with a misalignment of 0 mm – 80 mm at a 40 mm transfer distance. The radius of the Tx and Rx are 84.6 mm and 45.1 mm respectively. The measured PTE of the proposed design was better than 70% with a 0 mm to 50 mm transfer distance while the misalignment changing from 0 mm to 50 mm. The proposed system is much less sensitive to the transfer distance variation than the convention system and has a great potential for wireless charging applications.**

***Index Terms*— Bi-directional coils, differential coupling, strongly coupled magnetic resonances, wireless power transfer.**

I. INTRODUCTION

WIRELESS power transfer (WPT) systems via strongly coupled magnetic resonances (CMR) have shown a breakthrough in high-efficiency WPT applications [1], [2]. However, the resonant condition is a critical requirement of achieving maximum power transfer efficiency (PTE) between the transmitter (Tx) and receiver (Rx). The resonant condition of a given CMR-WPT system is usually fixed regarding the transfer position. Once the transfer position of the system varies from the optimum one, the PTE of the system will decrease significantly. In this work, the "distance" is defined as the space between the two planes where the Tx and Rx are located. The "horizontal misalignment" refers to the displacement of the center points of the Tx and Rx along the parallel planes. A shorter transfer distance (h) between Tx and Rx would cause over-coupling where the excessive coupling will split the resonant frequency. It weakens the power transfer at the original resonant frequency [3] – [5]. A larger transfer distance or horizontal misalignment (d) would reduce the coupling, leading to impedance mismatch which will degrade the PTE. Many applications such as the charging of biomedical bioelectronic device [6] – [12], electric vehicles [13], [14] and mobile electronics [15], [16] would require the flexibility of the transfer position and a high PTE simultaneously. Ideally, WPT systems should have a high PTE regardless of the transfer position variation [17], [18]. Recently, many methods have been presented to address this issue such as adaptive frequency tracking [1], [2], [19], [20] impedance control circuit [21], metamaterial [6], [7] and switching coils with different transfer distances [21], [22]. However, the added control or switching circuits will significantly increase the complexity of the system and reduce the overall system operating efficiency. Lee *et al* presented an antiparallel resonant loop structure to eliminate the frequency splitting by weakening the excessive coupling caused by the short transfer distance [23]. However, the maximum PTE will only be achieved at an optimal transfer distance, and the anti-misalignment ability was not discussed. Chen *et al* used the multiple-input and multiple-output concept with a multi-transmitter array system [24]. Assawaworrarit *et al* applied a nonlinear parity-time-symmetric circuit to achieve robust WPT. Excellent range-adaptive performance has been achieved [25]. But active circuits are needed, and the resonant frequency was adaptively changed to maintain high PTE. This can be a great limitation for WPT applications. A reconfigurable system is used to further increase PTE in conforming to charging device positions [26], [27]. However, very few passive solutions have been reported for a WPT system to achieve high PTE under both transfer distance variation and horizontal misalignment conditions simultaneously. Thus, how to design high-efficiency range-adaptive WPT systems without active control is still very challenging.

This paper aims to investigate a new method for solving this problem. This paper presents a planar Tx structure with multiple bi-directional sub-coils to maintain the resonant condition of the CMR-WPT system. This paper shows theoretically and demonstrates experimentally that the

Manuscript received March 14, 2019; revised June 13, 2019 and August 15, 2019; accepted September 11, 2019 (*Corresponding Authors: Jiafeng Zhou and Huapeng Zhao*).

Y. Zhuang, C. Xu, A. Chen, Y. Huang and J. Zhou are with the Department of Electrical Engineering and Electronics, University of Liverpool, Liverpool, L69 3GJ, U.K. (e-mail: sgyzhua2@163.com; c.xu12@liverpool.ac.uk; cholepjk@gmail.com; yi.huang@liverpool.ac.uk; jiafeng.zhou@liverpool.ac.uk).

H. Zhao is with the University of Electronic Science and Technology of China (e-mail: huapengzhao@uestc.edu.cn).

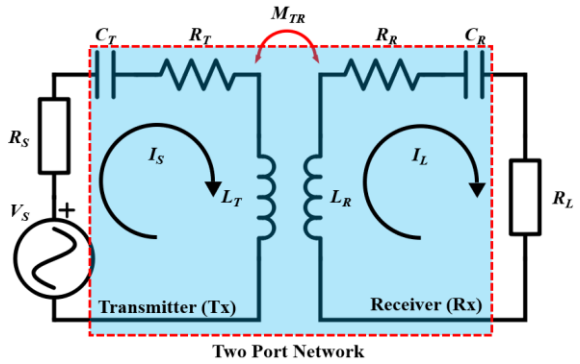

Fig. 1. An equivalent circuit of a typical two-coil MRC-WPT system.

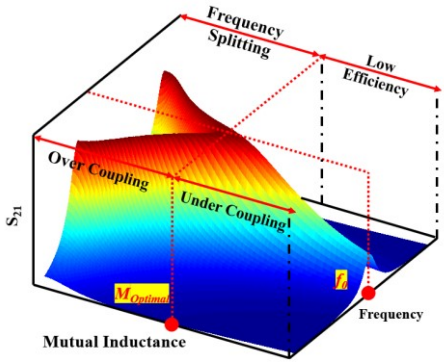

Fig. 2. Typical relationship among S_{21}, mutual inductance and resonant frequency.

proposed Tx structure can achieve a relatively constant mutual inductance between Tx and Rx over a broad range of transfer distance and misalignment variation without the need for any impedance tracking or active control circuits. The design concept will be described, and a robust mathematical model will be established for the optimization of the structure.

This paper is organized as follows. In section II, the basic operational principles of a two-coil MRC-WPT system are analyzed in detail. The challenges of high-efficiency range-adaptive WPT are identified. In Section III, the proposed multiple bi-directional resonant coils structure will be introduced with theoretical analysis and numerical simulation. A comparison with the conventional method is discussed. In Section IV, a prototype is fabricated. Measurement results are shown and analyzed. Conclusions are drawn in Section V to summarize the paper.

II. Theoretical Analysis

A. Two-Coil MRC-WPT Operating Principle

An equivalent circuit of a typical two-coil CMR-WPT system is depicted in Fig.1. R_S, R_L, L_T, L_R, R_T, R_R, C_T, C_R, and M_{TR} are the source resistance, load resistance, coils' self-inductance, coils' radiative and ohmic losses, resonating capacitor and mutual inductance of the Tx and Rx respectively. The radiative loss represents the portion of power radiated to the air during the power transfer process. It can be modelled as a lumped resistor dissipating power in the system. A CMR-WPT only use the near field to transfer power, where the wavelength is far larger than the physical dimension of the device. Hence, the radiative loss can be ignored [14]. For simplicity, assuming a lossless case, $R_T = R_R = 0\ \Omega$. The ratio of the received power on the load P_L and the input power P_S, namely PTE, is [5]:

$$\eta = \frac{P_L}{P_S} = |S_{21}|^2 \times 100\% \tag{1}$$

The node equations of the circuit based on Kirchhoff's voltage law can be built as:

$$\left(R_S + j\omega L_T + \frac{1}{j\omega C_T}\right) I_S - j\omega M_{TR} I_L = V_S \tag{2}$$

$$\left(R_L + j\omega L_R + \frac{1}{j\omega C_R}\right) I_L - j\omega M_{TR} I_S = 0 \tag{3}$$

where ω is the angular frequency of the system in rad/s. Combining (2) and (3), the current flowing through Rx can be obtained by:

$$I_L = \frac{j\omega M_{TR} V_S}{\omega^2 M_{TR}^{\ 2} + \left(j\omega L_T + \frac{1}{j\omega C_T} + R_S\right)\cdot\left(j\omega L_R + \frac{1}{j\omega C_R} + R_L\right)} \tag{4}$$

Then the S_{21} can be derived by:

$$\begin{aligned} S_{21} &= 2\frac{V_L}{V_S}\sqrt{\frac{R_S}{R_L}} = 2\frac{I_L R_L}{V_S}\sqrt{\frac{R_S}{R_L}} \\ &= \frac{2j\omega M_{TR}\sqrt{R_S R_L}}{M_{TR}^2\omega^2 + \left(j\omega L_T + \frac{1}{j\omega C_T} + R_S\right)\cdot\left(j\omega L_R + \frac{1}{j\omega C_R} + R_L\right)} \end{aligned} \tag{5}$$

If the circuit is operating at the resonant frequency ω_0 on both Tx and Rx side:

$$\omega_0 = \frac{1}{\sqrt{L_T C_T}} = \frac{1}{\sqrt{L_R C_R}} \tag{6}$$

then, (5) can be simplified to:

$$S_{21} = \frac{2j\omega_0 M_{TR}\sqrt{R_S R_L}}{M_{TR}^2\omega_0^{\ 2} + R_S R_L} \tag{7}$$

It can be observed form (7) that the power transferred to the load is dependent on the magnitude of the mutual inductance (coupling condition) between the Tx and Rx. To achieve the maximum PTE (for lossless condition S_{21} = 1), an optimal mutual inductance should be adopted critically to achieve the highest efficiency:

$$M_{Optimal} = \frac{\sqrt{R_S R_L}}{\omega_0} \tag{8}$$

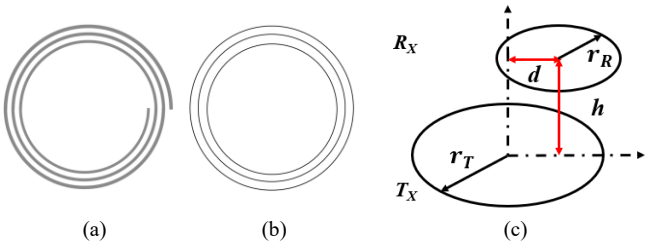

Fig. 3. (a) A multi-turn circular coil, (b) a set of single-turn filament coils, (c) simplified single-turn filamentary Tx/Rx coil configuration.

For a given source/load termination impedance, the relationship between S_{21}, the mutual inductance and the frequency can be plotted as shown in Fig. 2. The maximum efficiency operation at the desired resonating frequency can only be achieved when the mutual inductance is $M_{Optimal}$. When the system is operating at over coupling conditions, the resonating frequency will be split into two. The magnitude of S_{21} at the desired frequency will be degraded significantly due to the excessive coupling between Tx and Rx. On the other hand, when the system is working at under coupling conditions, the desired resonant frequency will be maintained but the PTE will drop dramatically due to the weak coupling. Hence, to transfer power with the maximum S_{21} at the desired resonating frequency, the mutual inductance must be maintained at $M_{Optimal}$.

B. Transfer Position and Mutual Inductance

The Tx and Rx of the MRC-WPT can be realized by using multi-turn circular coils connected in series with a capacitor to resonate. To calculate the mutual inductance between the Tx and Rx, a multi-turn coil can be simplified to a set of concentric single-turn coils. Every single turn can be further simplified to a filamentary coil [28] as shown in Fig. 3. N_T, N_R, r_{Ti} and r_{Rj} denote the number of turns, and radius of each single-turn coil for the Tx and Rx, respectively. The mutual inductance M_{ij} between the i^{th} single-turn Tx coil and j^{th} single-turn Rx coil can be expressed as a function of h and d, by the equation [28]:

$$M_{ij}\left(r_{Ti}, r_{Rj}, h, d\right) = \frac{\mu_0 \sqrt{r_{Ti} r_{Rj}}}{2\pi} \int_0^{2\pi} \frac{1 - \frac{d}{r_{Rj}} \cos(\phi)}{\zeta} \Lambda(k)\, d\phi \tag{9}$$

where the parameters in (9) can be expressed as:

$$\zeta = \left(1 + \frac{d^2}{r_{Rj}^2} - \frac{d}{r_{Rj}}\right)^{\frac{3}{4}} \tag{10}$$

$$\Lambda(k) = \left(\frac{2}{k} - k\right) K(k) - \frac{2}{k} E(k) \tag{11}$$

$$k = \sqrt{\frac{4\alpha\zeta^{\frac{4}{3}}}{\left(1 + \alpha\zeta^{\frac{4}{3}}\right)^2 + \beta^2}} \tag{12}$$

$$\alpha = \frac{r_{Rj}}{r_{Ti}}, \beta = \frac{h}{r_{Ti}} \tag{13}$$

where $\mu_0 = 4\pi \times 10^{-7}$ H/m is the magnetic constant, $K(k)$ and $E(k)$ are the complete elliptic integrals of the first and second kind, respectively [23]. The total mutual inductance between Tx and Rx with the number of the turns N_T and N_R can be calculated as:

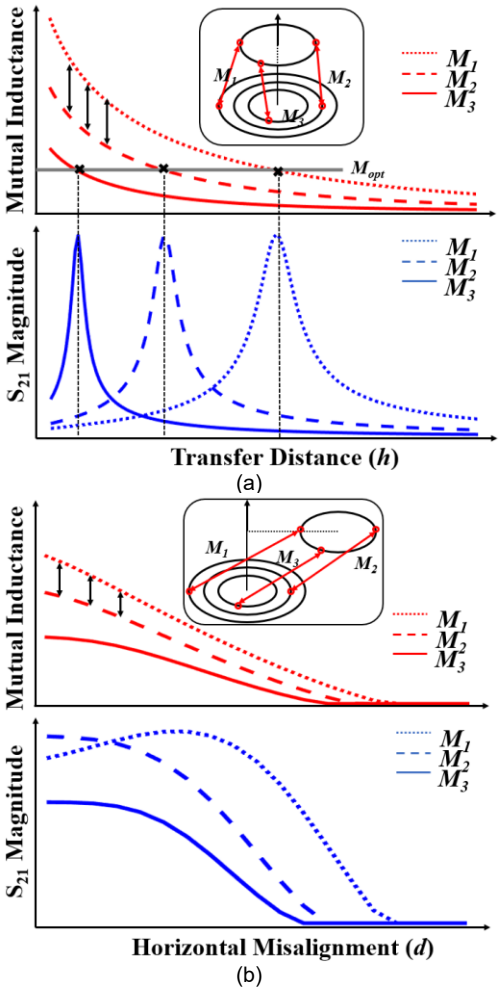

Fig. 4. Mutual inductance and S21 against the variation of (a) transfer distance, (b) horizontal misalignment for different Tx coils.

$$M_{TR} = \sum_{j=1}^{N_R} \sum_{i=1}^{N_T} M_{ij}(r_{Ti}, r_{Rj}, h, d) \tag{14}$$

Herein, for a given two-coil MRC-WPT system, there exists one set of values of h and d with which the system can achieve an optimum mutual inductance $M_{TR} = M_{Optimal}$, yielding the maximum S_{21} at the desired frequency. Variation in either the h or d is likely to degrade S_{21}.

III. Differential Coupling Design

A. Smooth Mutual Inductance against Transfer Distance

By combining (7) and (14), the relationship between S_{21} and the transfer position including both h and d can be obtained as shown in Fig. 4. It can be observed that when Tx coils with different sizes are coupled with the same Rx coil, the mutual inductance will generally decrease with the increase of either h or d. For any Tx size, there exists one set of h and d where the maximum S_{21} can be achieved.

For example, the mutual inductance between a Tx and an Rx can be calculated using (14). The mutual inductance of a

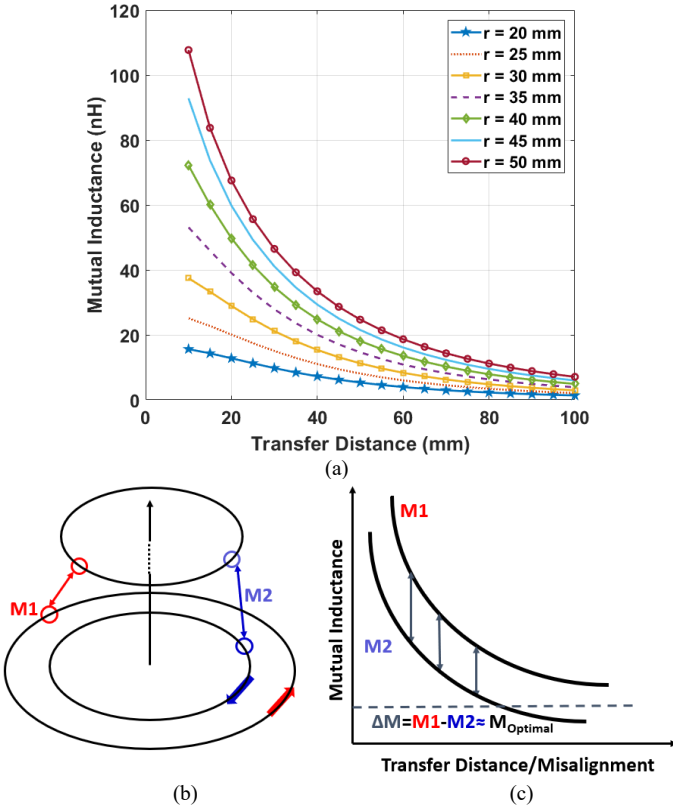

Fig. 5. (a) Mutual inductance variation with the transfer distance of different Tx sizes with the same Rx (b) Tx and Rx configuration, (c) Ideal case of mutual inductance variation against the transfer position of coils with different sizes.

single-turn Tx of different sizes as a function of h is illustrated in Fig. 5 (a). Although the magnitudes of the mutual inductances of different Tx are not identical, they follow a similar degradation trend. If the currents fed into two coils of different sizes are of opposite directions as shown in Fig. 5 (b), the total mutual inductance M_{total} can be depicted in Fig. 5 (c). The mutual inductance between each sub-coil in the Tx and the Rx decreases with the increase of the transfer distance or misalignment.

The sub-coils in the proposed Tx have two opposite directions. The sub-coils in the Tx of the clockwise direction and the Rx have an overall mutual inductance $M_{clockwise}$. The sub-coils in the Tx of the anti-clockwise direction and the Rx have an overall mutual inductance $M_{anti\text{-}clock}$. The total mutual inductance M_{total} will be the difference of $M_{clockwise}$ and $M_{anti\text{-}clock}$. Although both $M_{clockwise}$ and $M_{anti\text{-}clock}$ will decrease with the increase of the transfer distance or misalignment, by properly designing the sub-coils, M_{total} can be maintained relatively constant. An M_{total} that is robust against the transfer position can be realized. M_{total} can be optimized to approach $M_{Optimal}$ to achieve the desired coupling condition.

B. Bi-directional coil analysis and design

It should be noted that the concept has been used in microwave filter design. For coupled resonators in a filter, there exist two types of couplings: electrical coupling and magnetic coupling [29], [30]. The two couplings can be either weakening or strengthening each other, depending on the construction of the resonators. When the couplings are cancelling each other, it has been shown in a previous work [31] that the overall

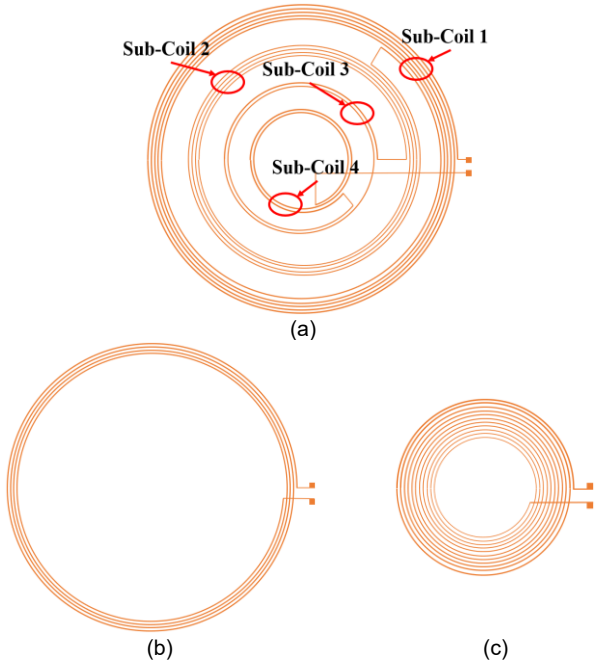

Fig. 6. Tx and Rx structures (a) proposed bi-directional Tx, (b) conventional unidirectional Tx, (c) unidirectional Rx.

coupling coefficient can be kept constant over a very wide range of distances. The magnitude of the overall coupling can be controlled by choosing proper dimensions for the resonators.

Once the optimal mutual inductance of the system is obtained by (8), the task resides in realising the desired mutual inductance by choosing a proper coil size, the number of sub-coils, the number of turns in each sub-coil for the Tx, and the current direction in each sub-coil. To ensure that current can flow in both directions, the Tx sub-coils are oriented in a bi-directional manner. The coils on the Rx are unidirectional. In the practical design, the Tx may consist of X sub-coils. Each sub-coil has N_{Ti} turns with an average radius of r_{Ti}. The X sub-coils are connected in series with adjacent sub-coils wound in opposite directions as shown in Fig. 5 (a). Four sub-coils are used in this design (X=4). A capacitor is connected to the coil to form a resonator. The total mutual inductance between the Tx and Rx of the proposed structure can be calculated as:

$$M_{total} = \sum_{n=1}^{X}\sum_{j=1}^{N_R}\sum_{i=1}^{N_{Tn}}(-1)^{n-1}M_{ij}(r_{Ti}, r_{Rj}, h, d) \tag{15}$$

The calculation of the total mutual inductance can be simplified by central approximation which uses the average coil size to represent each loop in the same sub-coil. Herein, (15) can be approximated as:

$$M_{total} \approx \sum_{n=1}^{X}(-1)^{n-1}N_R N_{Tn} M_n(r_{Tn}, r_R, h, d) \tag{16}$$

where M_n represents the mutual inductance between the n^{th} sub-coil in the Tx and the Rx. The turn number of the Rx coil is fixed in this work. The initial parameters of the turns are chosen empirically based on the desired transfer range and size requirement of the application. The flatness of the mutual

TABLE I: Design Parameters

Coil	Number of loops	Average radius (mm)	Self-Inductance (μH)	Capacitor (pF)	Unloaded Q	Direction
This work						
N_{T1}	5.2	84.6	20.9	11.7	63	Clockwise
N_{T2}	4.2	67.7				Anti-clockwise
N_{T3}	1.8	45.1				Clockwise
N_{T4}	2.2	33.9				Anti-clockwise
N_R	14	45.1	55.6	4.4	135	Clockwise
Type I						
N_T	5	45.1	7.1	34.3	101	N/A
N_R	5	45.1	7.1	34.3	101	N/A
Type II						
N_T	5	84.6	19.8	12.3	76	N/A
N_R	4	45.1	4.5	53.6	93	N/A

inductance against the transfer position can be obtained by optimising the number of turns in every sub-coil of the Tx. Other parameters, such as the width of each turn or the gap between adjacent turns, can also be taken into account for optimization if necessary. A differentiation-based method was used for the optimization. Because the slope of the mutual inductance curve against the transfer distance and misalignment are not identical, the optimization process against misalignment was carried out separately. If the total mutual inductance M_{total} changes slowly against the transfer distance h, the gradient of M_{total} against h should be very small, ideally close to zero. Assuming that the desired transfer distance is in the interval $[h_1, h_2]$, Y samples are selected in the interval $[h_1, h_2]$. At the m^{th} sample h_m, it is desired to achieve:

$$\sum_{n=1}^{X}(-1)^{n-1}N_R N_{Tn}\frac{dM_n(h)}{dh}\Big|_{h=h_m}=0 \tag{17}$$

On the other hand, let assume the transfer distance h is constant and now the total mutual inductance M_{total} (d) changes slowly against misalignment d, the differentiation of regards d should be close to zero. Thus, the differentiation of the mutual inductance regards d at the q^{th} sample d_q in the desired misalignment range $[d_1, d_2]$ should satisfy:

$$\sum_{n=1}^{X}(-1)^{n-1}N_R N_{Tn}\frac{dM_n(d)}{dd}\Big|_{d=d_q}=0 \tag{18}$$

For Y samples in the interval $[h_1, h_2]$, a matrix can be constructed based on (17), namely:

$$\overline{\overline{MH}}\,\overline{U}=\overline{0} \tag{19}$$

where $\overline{U}$ is a vector consisting of the number of loops for every Tx coil and $\overline{\overline{MH}}$ is a matrix with element in row m and column n given by:

$$M_{m,n}=(-1)^{n-1}N_R\frac{dM_n(h)}{dh}\Big|_{h=h_m} \tag{20}$$

The optimization of the mutual inductance against misalignment in the interval of $[d_1, d_2]$ can be carried out

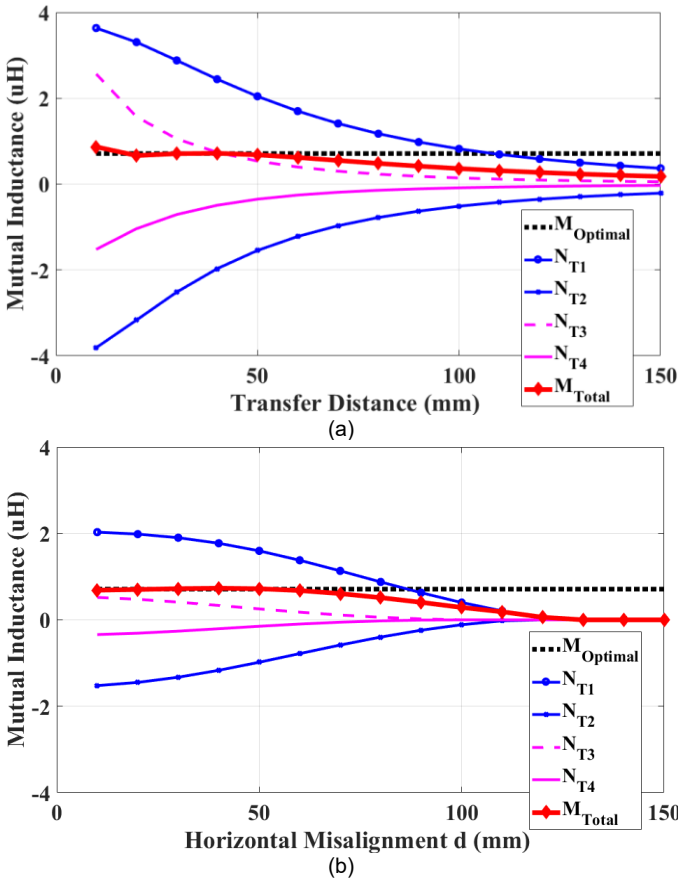

Fig. 7. Optimized flat mutual inductance against the position variation of (a) transfer distance and (b) horizontal misalignment of the proposed Tx structure.

similarly. For misalignment optimization, $\overline{\overline{MD}}$ is a matrix whose element in row q and column n can be expressed by:

$$M_{m,n}=(-1)^{n-1}N_R\frac{dM_n(d)}{dd}\Big|_{d=d_q} \tag{21}$$

Now, the optimal loops number for each sub-coil can be found by solving the following equations:

$$\begin{bmatrix} N_R\frac{dM_1(h)}{dh}\Big|_{h=h_1} & \cdots & {}^{-1}N_R\frac{dM_n(h)}{dd}\Big|_{h=h_1} \\ \vdots & \ddots & \vdots \\ N_R\frac{dM_1(h)}{dh}\Big|_{h=h_m} & \cdots & {}^{-1}N_R\frac{dM_n(h)}{dh}\Big|_{h=h_m} \end{bmatrix}\begin{bmatrix} N_{T1} \\ \vdots \\ N_{Tn} \end{bmatrix}=\begin{bmatrix} 0 \\ \vdots \\ 0 \end{bmatrix}$$

$$\begin{bmatrix} N_R\frac{dM_1(d)}{dd}\Big|_{d=d_1} & \cdots & {}^{-1}N_R\frac{dM_n(d)}{dd}\Big|_{d=d_1} \\ \vdots & \ddots & \vdots \\ N_R\frac{dM_1(d)}{dd}\Big|_{d=d_q} & \cdots & {}^{-1}N_R\frac{dM_n(d)}{dd}\Big|_{d=d_q} \end{bmatrix}\begin{bmatrix} N_{T1} \\ \vdots \\ N_{Tn} \end{bmatrix}=\begin{bmatrix} 0 \\ \vdots \\ 0 \end{bmatrix} \tag{22}$$

$$\sum_{n=1}^{X}(-1)^{n-1}N_R N_{Tn}M_n(r_{Tn},r_R,h,d)=M_{Optimal}$$

Finally, the optimal solution can be obtained for the system to achieve the desired mutual inductance for the desired range $[h_1, h_2]$ and $[d_1, d_2]$.

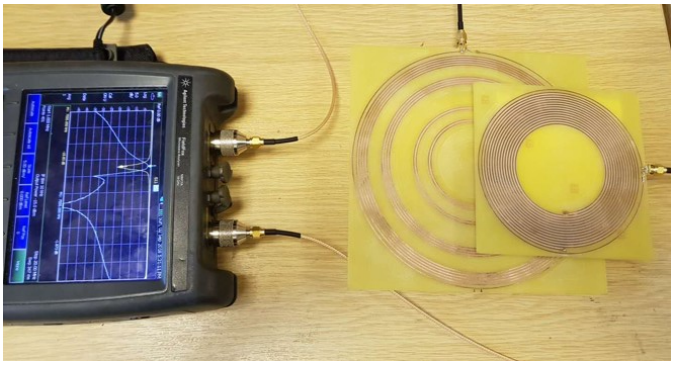

Fig. 8. A photograph of the measurement setup.

C. Numerical Calculation

To evaluate the proposed method, one prototype was designed. The desired optimal ranges for transfer distance and misalignment are set to be h_1 = 10 mm, h_2 = 50 mm and d_1 = 0 mm, d_2 = 50 mm respectively. The number of samples used in (15) is 5 for both the transfer distance and misalignment. The parameters obtained by calculation via (15) – (22) are listed in Table 1.

The anti-misalignment feature of the proposed system is optimised at h = 50 mm. The mutual inductance between the Rx and each sub-coil in Tx, and total mutual inductance of the system against the transfer distance and horizontal misalignment are calculated using (9) and (14), respectively. The calculated results are shown in Fig. 7. For both the transfer distance varying from 10 mm to 50 mm and the misalignment varying from 0 mm to 50 mm, the total mutual inductances are very constant against the transfer position variation and close to the optimal value. This validates the proposed design method. A high-efficiency range-adaptive CMR-WPT system can be realised.

IV. Implementation and Measurements

To validate the proposed CMR-WPT structure and the design method, a prototype has been fabricated on an FR4 substrate with parameters listed in Table I. The proposed Tx and Rx structures are shown in Fig. 6 (a) and (c) respectively. Furthermore, two conventional unidirectional CMR-WPT systems have been built, namely, Type I and Type II with parameters shown in Table I, to compare the performance of the proposed work. Type I uses a Tx with an identical structure to the Rx. Type II uses a Tx with the same size as the proposed structure but without using bi-directional sub-coils as shown in Fig. 6 (b). All three systems use an Rx of the same size. The windings of the three Rx are different due to that the resonant conditions are different. The port terminations of the WPT systems were chosen to be 50 Ω for simplicity. A vector network analyser (VNA) and 50 Ω cables were used for the measurement. The S_{21} performance is evaluated by the two-port 50 Ω VNA. A photograph of the measurement set-up is shown Fig. 8.

The measured S_{21} (dB) of the proposed system and the conventional systems are presented in Fig. 9. The value of h is varied from 10 mm to 150 mm (10 -110 mm for Type-I due to that S_{21} is too small with a larger distance). The proposed

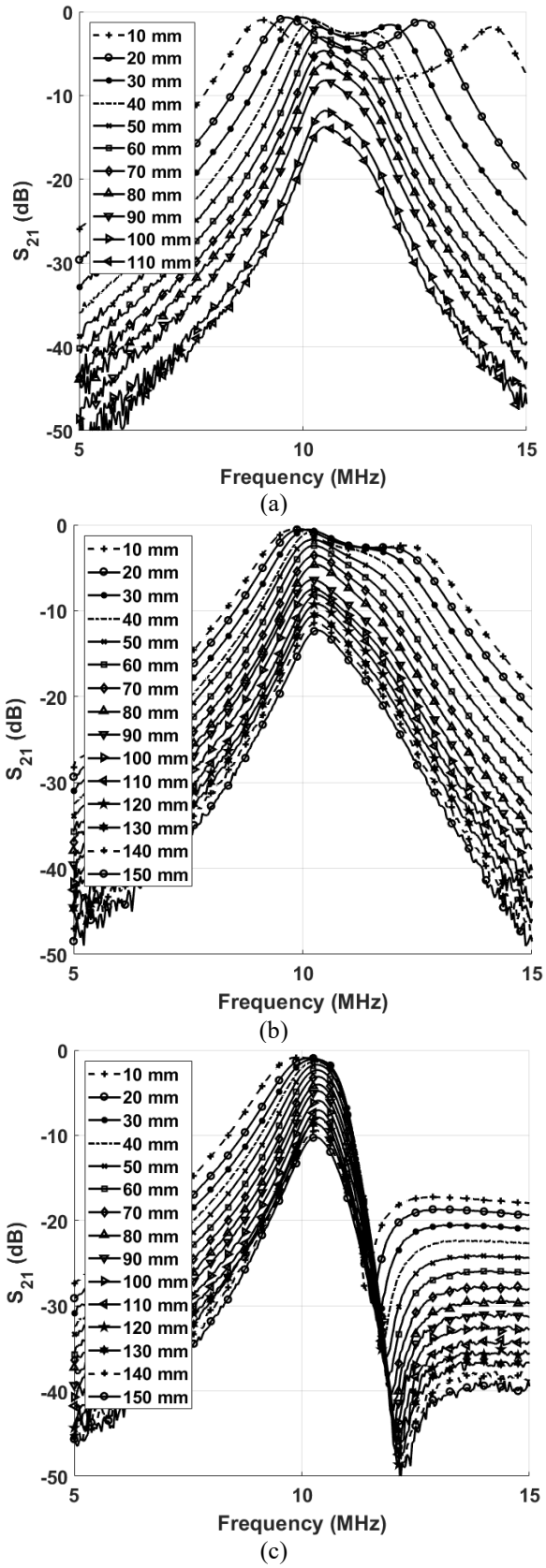

Fig. 9. Measured S_{21} against frequency with the variation of h of (a) Type-I, (b) Type-II, (c) the proposed system.

system shows the capability of avoiding the frequency splitting phenomena while the conventional designs have shifted resonant frequencies at shorter transfer distances. The

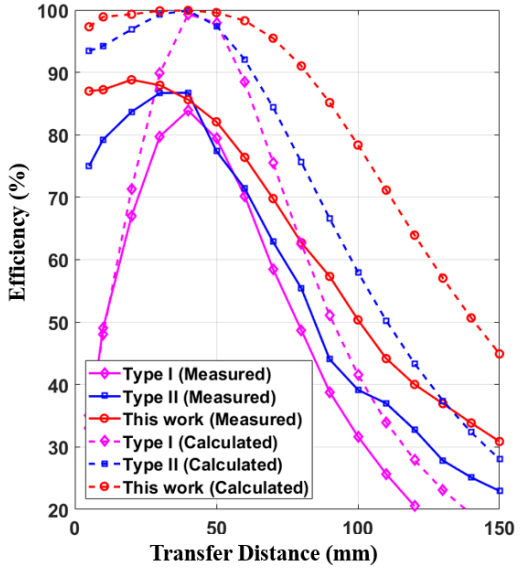

(a)

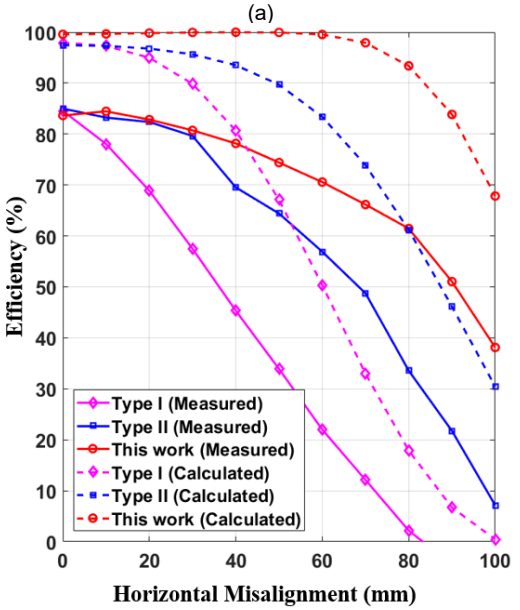

(b)

Fig. 10. Comparison of the measured PTE of the proposed system with conventional designs against (a) transfer distance (d = 0 mm), (b) horizontal misalignment (h = 40 mm).

measured S_{21} at the desired resonant frequency (10.3 MHz in this work) against the transfer distance (without misalignment d = 0 mm) is depicted in Fig. 10 (a). The conventional designs were able to achieve the maximum S_{21} only at h = 40 mm. The S_{21} drops fast when the transfer distance deviates from the optimum one. The proposed system has a significantly improved efficiency with both shorter and longer transfer distances. The S_{21} of the proposed design has a much slower degradation slope compared to the conventional designs. The proposed design achieved a S_{21} better than 70% with a transfer distance varying from 0 mm to 70 mm, or better than 40% with the transfer distance changing from 0 mm to 130 mm. The results validate that the proposed system is robust against the transfer distance variation.

The measured PTE at the desired resonant frequency against the d varying from 0 mm to 100 mm is depicted in Fig. 10 (b). Here h = 40 mm was chosen because Type I and Type II

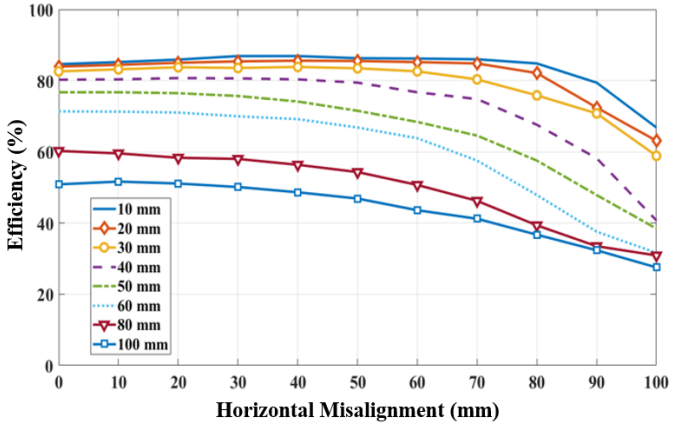

Fig. 11. Measured PTE performance against the horizontal misalignment with different transfer distances.

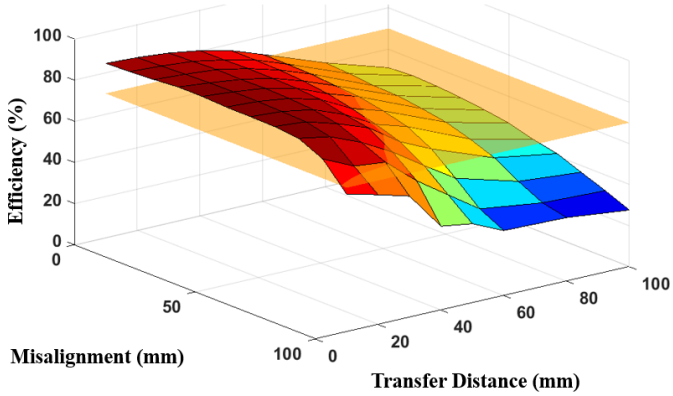

Fig. 12. Measured PTE performance with the transfer position variation with a reference efficiency of 70%.

designs can achieve the highest PTE at this transfer distance. The measured PTE of the Type I design drops rapidly. The Type II system can maintain a slightly slower degradation when d is smaller than 30 mm. Once d is comparable to the radius of the Rx, the deterioration of the Type II PTE is dramatic. The proposed system achieves a much slower PTE decrease against d compared with the conventional systems. The proposed design can maintain a PTE better than 40% with the misalignment changing from 0 mm to 100 mm. The results prove that the proposed system has a better robustness to the horizontal misalignment compared with Type I and II systems. Although the highest PTE has not been improved by the proposed system compared with the other designs, the PTE degradation has been significantly improved.

Further investigation was carried out to demonstrate the anti-misalignment ability of the proposed system with other transfer distances. The measured PTE of the proposed system against both the transfer distance and misalignment are plotted in Fig. 11. When the transfer distance is smaller than 40 mm, the PTE can be maintained above 70% with the misalignment varying from 0 mm to 70 mm. Although the anti-misalignment ability will not be as good when the transfer distance further increases, the PTE has been kept better than 30% with a misalignment of 100 mm at the distance of 100 mm as shown in Fig. 11. The performance of the proposed system against the transfer position variation is shown in Fig. 12 with a 70% S_{21}

reference plane. The proposed system has achieved a PTE better than 70% with transfer distances from 0 mm to 50 mm and misalignment from 0 mm to 50 mm. The measured results show a great potential of the proposed system in applications where the flexibility of transfer position and a high efficiency are critical.

V. Conclusion

WPT systems using magnetic couplings are usually susceptible to transfer distance and alignment since the coupling between the transmitting and receiving coils is highly position-dependent. Once the transfer position deviates from the optimum one, the coupling will be either too strong or too weak which results in transfer efficiency degradation. This paper presents a new transmitter structure consisting of multiple sub-coils oriented in opposite directions. The coupling between the TX and Rx is kept relatively constant over an extensive range of transfer distance and alignment. A prototype developed using the proposed method is able to achieve a PTE of 88% - 70% with the transfer distance varying from 5 mm to 70 mm and a PTE of 85% - 60% with the misalignment changing from 0 mm – 80 mm at a 40 mm transfer distance. The diameters of the transmitter and receiver are 84.6 mm and 45.1 mm respectively. The measured PTE of the proposed design can be kept better than 70% with a transfer distance varying from 5 mm to 50 mm and the misalignment from 0 mm to 50 mm. One suitable application of the proposed system is the wireless charging or portable devices such as smartphones. Because the proposed system is robust against the transfer position variation between the transmitter and receiver, it can enable high-efficiency charging while the device is being used, as long as it is near the transmitter. The unloaded Q of the resonators on a PCB in the proposed design is not very high. For applications that require a higher power transfer efficiency than our current design, the coils can be fabricated using wound wires to improve Q and efficiency. Furthermore, the proposed structure can be scaled up/down for other applications such as the wireless charging of drones, electrical vehicles, wearable devices and implantable devices.

References

[1] A. Kurs, A. Karalis, R. Moffatt, J. D. Joannopoulos, P. Fisher and M. Soljacic, "Wireless power transfer via strongly coupled magnetic resonances," *Science.*, vol. 317, no.5834, pp. 83-86, Jul. 2007.

[2] A. P. Sample, D. T. Meyer, and J. R. Smith, "Analysis, experimental results, and range adaptation of magnetically coupled resonators for wireless power transfer," *IEEE Transactions on Industrial Electronics.*, vol. 58, DOI: 10.1109/TIE.2010.2046002, no. 2, pp. 544–554, Feb. 2011.

[3] S. Jeong, D. H. Kim and *et al* , "Smartwatch strap wireless power transfer system with flexible PCB coil and shielding material," *IEEE Trans. Ind. Electron., Early Access*, DOI 10.1109/TIE.2018.2860534, Aug. 2018.

[4] W. Q. Niu, J. X. Chu, W. Gu and A. D. Shen, "Exact analysis of frequency splitting phenomena of contactless power transfer systems," *IEEE Transactions on Circuit and System I: Regular Papers*., vol. 60, DOI 10.1109/TCSI.2012.2221172, no. 6, pp. 1670-1677, Jun. 2013.

[5] Y. Zhang and Z. Zhao, "Frequency splitting analysis of two-coils resonant wireless power transfer," *IEEE Antennas and Wireless Propagation Letters.*, vol. 13, pp. 400-402, Feb. 2014.

[6] L. Li, H. Liu, H. Zhang and W. Xue, "Efficient wireless power transfer system integrating with metasurface for biological applications," *IEEE Trans. Ind. Electron*., vol. 65, no. 4, pp. 3230–3239, Apr. 2018.

[7] G. Lipworth *et al.,* "Magnetic Metamaterial superlens for increased range wireless power transfer," *Scientific Reports.,* vol. 4**,** no. 3642, Jan. 2014.

[8] D. R. Agrawal *et al.,* "Conformal phased surfaces for wireless powering of bioelectronic microdevices," *Nature Biomedical Engineering.,* vol. 1, no. 43, Mar. 2017.

[9] P. Abiri *et al.,* "Inductively powered wireless pacing via a miniature pacemaker and remote stimulation control system," *Scientific Reports.,* vol. 7, no. 6180, Jul. 2017.

[10] K. L. Montgomery *et al.,* "Wirelessly powered, fully internal optogenetics for brain, spinal and peripheral circuits in mice," *Nature Methods.,* vol. 12, pp. 969-974, Aug. 2015.

[11] H. Mei and P. P. Irazoqui, "Miniaturizing wireless implants," *Nature Biotechnology.,* vol. 32, pp. 1008-1010, Oct. 2014.

[12] K. Yamagishi *et al.,* "Tissue-adhesive wirelessly powered optoelectronic device for metronomic photodynamic cancer therapy," *Nature Biomedical Engineering.,* vol. 3, pp. 27-36, Jul. 2018.

[13] K. Aditya and S. S. Williamson, "Design guidelines to avoid bifurcation in a series-series compensated inductive power transfer system," *IEEE Trans. Ind. Electron*, vol. 66, DOI 10.1109/TIE.2018.2851953, no. 5, pp. 3973-3982, Jul. 2018.

[14] J. Liu, K. W. Chan, C. Y. Chung, N. H. L. Chan, M. Liu and W. Xu, "Single-stage wireless-power-transfer resonate converter with boost bridgeless power-factor-correction rectifier," *IEEE Trans. Ind. Electron.*, vol. 65, DOI 10.1109/TIE.2017.2745471, no. 3, pp. 2145–2155, Apr. 2018.

[15] C. Jiang, K. T. Chau, Y. Leung, C. H. T. Lee and W. Han, "Design and analysis of wireless ballastless fluorescent lighting," *IEEE Trans. Ind. Electron.,* vol. 66, DOI 10.1109/TIE.2017.2784345, no. 5, pp. 4065-4074, Dec. 2017.

[16] Y. Zhang and Z. Zhao, "Frequency splitting analysis of four-coils resonant wireless power transfer," *IEEE Transactions on Industry Applications.*, vol. 50, DOI 10.1109/TIA.2013.2295007, no. 4, pp. 2436-2445, Dec. 2013.

[17] H. Nguyen and J. Agbinya, "Splitting frequency diversity in wireless power transmission," *IEEE Transactions on Power Electronics.*, vol. 30, DOI 10.1109/TPEL.2015.2424312, no. 11, pp. 6088-6096, Apr. 2015.

[18] R. Huang, B. Zhang, D. Qiu and Y. Zhang, "Frequency splitting phenomena of magnetic resonant coupling wireless power transfer," *IEEE Transactions on Magnetics*, vol. 50, DOI 10.1109/TMAG.2014.2331143, no. 11, Nov. 2014.

[19] W. Fu, B. Zhang, and D. Qiu, "Study on frequency-tracking wireless power transfer system by resonant coupling," in *Proc. IEEE IPEMC*, DOI: 10.1109/IPEMC.2009.5157857, May 2009.

[20] A. Abid *et al*., "Wireless power transfer to millimeter-sized gastrointestinal electronics validated in a swine model," *Scientific Reports*., vol. 7, no. 46746, Apr. 2017.

[21] T. C. Beh, T. Imura, M. Kato, and Y. Hori, "Basic study of improving efficiency of wireless power transfer via magnetic resonance coupling based on impedance matching," in *Proc. IEEE International Symposium on Industrial Electronics.*, DOI:10.1109/ISIE.2010.5637484. Jul. 2010.

[22] J. Kim and J. Jeong, "Range-adaptive wireless power transfer using multiloop and tunable matching techniques*," IEEE Trans. Ind. Electron*., vol. 62, no. 10, pp. 6233–6241, Oct. 2015.

[23] W. S. Lee, W. I. Son, K. S. Oh, and J. W. Yu, "Contactless energy transfer systems using antiparallel resonant loops*," IEEE Trans. Ind. Electron*., vol. 60, no. 1, pp. 350–359, Jan. 2013.

[24] X. M. Chen, X. Wang and X. F. Chen, "Energy-efficient optimization for wireless information and power transfer in large-scale MIMO systems employing energy beamforming," *IEEE Wireless Communications Letters*, vol. 2, DOI 10.1109/WCL.2013.092813.130514, pp. 667-670, Oct. 2013.

[25] S. Assawaworrarit, X. F. Yu and S. H. Fan, "Robust wireless power transfer using a nonlinear parity-time-symmetric circuit," *Nature*., vol. 546, pp. 387-390, Jun. 2017.

[26] X. Li, C. Y. Tsui and W. H. Ki, "A 13.56 MHz wireless power transfer system with reconfigurable resonant regulating rectifier and wireless power transfer control for implantable medical devices," *IEEE Journal of Solid-state Circuits*., vol. 50, DOI 10.1109/JSSC.2014.2387832, no. 4, pp. 978-989, Feb. 2015.

[27] Z. Dang, Y. Cao and J. Qahouq, "Reconfigurable magnetic resonance-coupled wireless power transfer system," *IEEE Transactions on Power Electronics*., vol. 30, DOI 10.1109/TPEL.2015.2422776, no. 11, pp. 6057-6069, Nov. 2015.

[28] C. Akyel, S. I. Babic and M. M. Mahmoudi, "Mutual inductance calculation for non-coaxial circular air coils with parallel axes," *Progress in Electromagnetic Research*., vol. 91, pp. 287–301, 2009.
[29] J. S. Hong, *Microstrip Filters for RF / Microwave Applications*, 2nd ed, John Wiley & Sons, 2011.
[30] J. S. Hong and M. J. Lancaster, "Couplings of microstrip square open-loop resonators for cross-coupled planar microwave filters," *IEEE Transactions on Microwave Theory and Techniques*., vol. 44, no. 11, pp. 2099-2109 ,1996.
[31] Y. Di, P. Gardner, P. Hall, H. Ghafouri-Shiraz and J. Zhou, "Multiple-coupled microstrip hairpin-resonator filter," *IEEE Microwave and Wireless Components Letters*., vol. 13, no. 12, pp. 532-534, 2003.

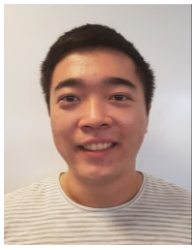

Yuan Zhuang was born in Baoding, Hebei, China, in 1991. He received the B.Eng degree (Hons) in telecommunication engineering from Xi'an Jiao Tong Liverpool University, Suzhou, China and University of Liverpool in 2014, and PhD degree in Electrical Engineering and Electronics from University of Liverpool, Liverpool, United Kingdom in July 2019. He is a research assistant with the University of Liverpool, Liverpool, UK.

His research interests include microwave power amplifiers, filters, electromagnetic energy harvesting and wireless power transfer.

Anqi Chen was born in Jingdezhen, China. She received a joint B.Eng. degree in Telecommunication Engineering from Xi'an Jiao Tong Liverpool University, Suzhou, China, and Electrical Electronics Engineering from University of Liverpool, Liverpool, UK, in 2014. She received a Ph.D. degree with the University of Liverpool in Electrical & Electronic Engineering, Liverpool, UK.

Her main research interest is RF passive circuit including broadband power divider designs and millimeter-wave filter/diplexer designs.

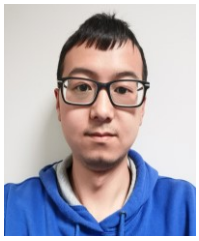

Chen Xu was born in Baoji, China in 1994. He received the B.Eng. (Hons.) degree in electrical engineering from the XJTLU, Suzhou, China, and University of Liverpool, Liverpool, UK, in 2016. He is currently pursuing the Ph.D. degree at department of Electrical engineering and electronics, University of Liverpool, Liverpool, UK.

His current research interests include wireless power transfer for portable devices and electrical field energy harvesting of high voltage power line.

Yi Huang (S'91 – M'96 – SM'06) received BSc in Physics (Wuhan University, China) in 1984, MSc (Eng) in Microwave Engineering (NRIET, Nanjing, China) in 1987, and DPhil in Communications from the University of Oxford, UK in 1994.

He has been conducting research in the areas of wireless communications, applied electromagnetics, radar and antennas since 1987. His experience includes 3 years spent with NRIET (China) as a Radar Engineer and various periods with the Universities of Birmingham, Oxford, and Essex at the UK as a member of research staff. He worked as a Research Fellow at British Telecom Labs in 1994, and then joined the Department of Electrical Engineering & Electronics, the University of Liverpool, UK as a Faculty in 1995, where he is now a full Professor in Wireless Engineering, the Head of High Frequency Engineering Group and Deputy Head of Department.

Prof Huang has published over 350 refereed papers in leading international journals and conference proceedings, and authored Antennas: from Theory to Practice (John Wiley, 2008) and Reverberation Chambers: Theory and Applications to EMC and Antenna Measurements (John Wiley, 2016). He has received many research grants from research councils, government agencies, charity, EU and industry, and is a recipient of 8 awards (e.g. BAE Systems Chairman's Award 2017, IET Innovation Award 2018, and Best Paper Awards), and served on a number of national and international technical committees and been an Editor, Associate Editor or Guest Editor of five international journals. He has been a keynote/invited speaker and organiser of many conferences and workshops (e.g. IEEE iWAT2010, LAPC2012 and EuCAP2018). He is at present the Editor-in-Chief of Wireless Engineering and Technology, Associate Editor of IEEE Antennas and Wireless Propagation Letters, UK and Ireland Rep to European Association of Antenna and Propagation (EurAAP), a Senior Member of IEEE, a Fellow of IET, and Senior Fellow of HEA.

Huapeng Zhao (S'08–M'12) was born in Hebei Province, P. R. China, in 1983. He received the Bachelor's and Master's degrees in Electromagnetic Field and Microwave Technology from the University of Electronic Science and Technology of China, Chengdu, P. R. China, in July 2004, and March 2007, respectively, and the Ph.D. degree in Communication Engineering from the Nanyang Technological University, Singapore, in June 2012. He was a Scientist with the Institute of High-Performance Computing, Agency for Science, Technology and Research (A*STAR), Singapore, from August 2011 to December 2015. Since December 2015, he has been an Associate Professor with the School of Electronic Science and Engineering at the University of Electronic Science and Technology of China, Chengdu, P. R. China.

Dr. Zhao has authored or coauthored over 100 technical papers published in international journals or conferences. He was the Technical Program Committee Chair of 2016 Asia Wireless Power Transfer Workshop, and the member of Organizing Committee/Technical Program Committee of several international conferences. He currently severs the Associate Editor of IEEE ACCESS and was a Guest Editor of International Journal of Antennas and Propagation. His current research interests include system-level electromagnetic analysis and design, and signal and data processing techniques in electromagnetics. He received the 2016 IEEE Asia–Pacific Electromagnetic Compatibility Young Scientist Award and the 2014 URSI Young Scientist Award.

Jiafeng Zhou received a B.Sc. degree in Radio Physics from Nanjing University, Nanjing, China, in 1997, and a Ph.D. degree from the University of Birmingham, Birmingham, U.K., in 2004. His doctoral research concerned high-temperature superconductor microwave filters.

From July 1997, for two and a half years he was with the National Meteorological Satellite Centre of China, Beijing, China, where he was involved with the development of communication systems for Chinese geostationary meteorological satellites. From August 2004 to April 2006, he was a Research Fellow with the University of Birmingham, where his research concerned phased arrays for reflector observing systems. Then he moved to the Department of Electronic and Electrical Engineering, University of Bristol, Bristol, U.K until August 2013. His research in Bristol was on the development of highly efficient and linear amplifiers. He is now with the Department of Electrical Engineering and Electronics, University of Liverpool, Liverpool, UK.

His current research interests include microwave power amplifiers, filters, electromagnetic energy harvesting and wireless power transfer.